Journal of Materials Chemistry C

ROYAL SOCIETY OF CHEMISTRY

PAPER

View Article Online
View Journal | View Issue

Cite this: J. Mater. Chem. C, 2024, 12, 11426

Modulating organic functional groups in stimuli-responsive luminescent antimony chlorides†

Yi Liu,‡[acd] Dan-Dan Huang,‡[acd] Zhi-Zhuan Zhang,[c] Hao-Wei Lin,[ac] Ke-Zhao Du,[b] Ze-Ping Wang*[c] and Xiao-Ying Huang*[cd]

Received 2nd April 2024,
Accepted 16th June 2024

DOI: 10.1039/d4tc01344a

rsc.li/materials-c

Stimuli-responsive inorganic–organic hybrid metal halides (IOMHs) have shown great potential in sensing, information encryption and anti-counterfeiting, *etc.* However, the stimuli-responsive behavior based on the regulation of the functional groups in organic species is still blank in IOMHs. Herein, three zero-dimensional (0-D) antimony-based IOMHs with different functional groups in the organic cations are reported, namely $[AOEMIm]_3SbCl_6$ (**1**, AOEMIm = 1-acetoxyethyl-3 methylimidazolium), $[HOOCMMIm]_3SbCl_6{\cdot}3(OOCMMIm)$ (**2**, HOOCMMIm = 1-carboxymethyl-3-methylimidazolium) and $[HOOCMMIm]_3SbCl_6$ (**3**). Photophysical characterizations show that **1**, **2** and **3** exhibit typical self-trapped exciton triplet broadband emission, peaking at 610, 510 and 525 nm under excitation of 365 nm, 375 nm and 345 nm, respectively. Under the H_2O stimulation, the organic groups in the crystal structures undergo a mutual transformation, that is, from acetoxyethyl or carboxyl to a mixture of carboxyl and deprotonated carboxyl. Accordingly, the organic group switching is accompanied by a solid–solid transformation from **1** or **2** to **3** crystals. The intrinsic mechanism for the phase transition is expounded as well. Due to the obvious luminescence change from yellow-green emission (**3**) to green emission (**2**), **3** is further applied in the detection of trace water in organic solvents. The water detection limit in tetrahydrofuran (THF) is as low as 0.3% v/v. This study provides a new avenue for the construction of stimuli-responsive IOMHs.

Introduction

Inorganic–organic hybrid metal halides (IOMHs) have attracted much attention in the fields of lighting, imaging, anti-counterfeiting, ferroelectrics, and solar cells due to their simple synthesis methods, excellent luminescence properties, and variable structures.[1–13] Typical IOMHs have the chemical formula A_mBX_n (A = organic cation, B = metal ion, X = halide anion).[14] The composition and ionic structure characteristics of IOMHs dictate relatively weak interactions between cations and anions, leading to the formation of a soft lattice and chemical reactivity.[15] Therefore, IOMHs are susceptible to structural transformations after regulating external factors such as temperature,[16–20] humidity[21–25] and pressure.[26] The structural transformation can lead to strong fluorescence changes, such as fluorescence enhancement (on), diminution (off) or luminescence colour shift,[22,23,27,28] which makes IOMHs an ideal

[a] College of Chemistry, Fuzhou University, Fuzhou 350108, P. R. China
[b] Fujian Provincial Key Laboratory of Advanced Materials Oriented Chemical Engineering, Fujian Normal University, 32 Shangsan Road, Fuzhou 350007, P. R. China. E-mail: duke@fjnu.edu.cn
[c] State Key Laboratory of Structural Chemistry, Fujian Institute of Research on the Structure of Matter, Chinese Academy of Sciences, Fuzhou, Fujian 350002, P. R. China. E-mail: wzping@fjirsm.ac.cn
[d] Fujian College, University of Chinese Academy of Sciences, Fuzhou 350002, P. R. China. E-mail: xyhuang@fjirsm.ac.cn

† Electronic supplementary information (ESI) available. CCDC 2341218, 2344297,2341219. For ESI and crystallographic data in CIF or other electronic format see DOI: https://doi.org/10.1039/d4tc01344a

‡ Yi Liu and Dan-Dan Huang contributed equally to this work.

Ke-Zhao Du

Ke-Zhao Du received a PhD degree in 2013 from Fujian Institute of Research on the Structure of Matter, Chinese Academy of Sciences, China under the supervision of Prof. Xiaoying Huang. After that, he worked as a postdoctoral researcher in Nanyang Technological University, Singapore and Duke University, USA. In 2018, he joined Fujian Normal University, China as a professor. His research interest focuses on the crystal structure–property relationship study of metal halides and their applications for energy transformation.

class of stimuli-responsive luminescent materials.

However, most of the previously reported stimuli-responsive structural changes of IOMHs occur in inorganic components or lattices. That is, the external stimulation significantly changes the bond length and bond angle of the inorganic components,[29,30] the coordination number of metal ions, the coordination/insertion of the guest molecules, or the dimensional change of BX_n^{m-}.[31–42] For example, Xiao *et al.*[43] reported that the bond length and bond angle of Sn^{2+}-IOMHs $C_4N_2H_{14}SnBr_4$ change significantly with increasing pressure, resulting in a larger dipole moment and higher structural and excited state distortion. Peng *et al.* found that the hydrogen bond strength in $[EtPPh_3]_2[SbCl_5]$ can be influenced by diverse organic functional groups upon exposure to different organic gases. Consequently, the emission of the $[SbCl_5]^{2-}$ unit is changed depending on their different distortion, resulting in solvatochromic and thermochromic photoluminescence (PL).[4] Zang *et al.* reported the conversion of a green-emitting complex, $C_6N_2H_{16}MnBr_4$, into a non-emissive hydrated phase, $C_6N_2H_{16}MnBr_4(H_2O)_2$, by absorbing coordinated water molecules. The reversible crystal phase transition can switch the PL as well.[33] As we know, most phase transition cases are involved with the isomerisation of organic cations in IOMHs.[25,44,45] For example, Zhang *et al.* reported that chiral *β*-$[Bmmim]_2SbCl_5$ transforms into achiral *α*-$[Bmmim]_2SbCl_5$ by crystalline phase recognition, resulting in a domino phase transition accompanied by photoluminescence switching.[46] However, the stimuli-responsive organic species reconstruction is still blank in OIMHs, which would broaden the research area in stimuli-responsive IOMHs.

Keeping this in mind, we selected organic cations with special functional groups to synthesize three IOMHs to study the organic reconstruction induced switching on structure and PL, namely $[AOEMIm]_3SbCl_6$ (**1**, AOEMIm = 1-acetoxyethyl-3-methylimidazolium) $[HOOCMMIm]_3SbCl_6{\cdot}3(OOCMMIm)$ (**2**,[47] HOOCMMIm = 1-carboxymethyl-3-methylimidazolium), and $[HOOCMMIm]_3SbCl_6$ (**3**). Benefitting from the potential post-synthetic modification behaviour of cationic functional groups, external stimuli can be used to achieve the reconstruction of organic moieties, resulting in a series of controllable and stepwise structural transformations. Both **1** and **3** can respond to humidity stimulation and eventually change to **2**, while **2** is reversibly converted to **3** under HCl and $SbCl_3$ atmospheres. The apparent luminescence switching during the structural transformation makes **2** and **3** ideal candidates for fluorescent humidity sensors. Study shows that **3** can detect trace water in organic solvents with a detection limit as low as 0.3% v/v.

Results and discussion

Synthesis and crystal structural description

Single crystals of **1** were synthesized by an ionothermal reaction method. Using the same raw materials, **2** and **3** were synthesized by different reactant ratios and solvents (see ESI† for detailed information). The discrete anionic units $[SbCl_6]^{3-}$ of the three compounds were surrounded by different cations (and neutral molecules in **2**) to form a 0-D structure. The three compounds form a three-dimensional supramolecular framework based on hydrogen bonding forces (Fig. 1d–f). Detailed crystallographic and supramolecular interaction data for **1**, **2**, and **3** are listed in Tables S1–S3 (ESI†).

1 crystallizes in an orthorhombic crystal system with the space group of *Pbca* and the cell parameters are a = 20.4908(3) Å, b = 16.2409(3) Å, c = 21.6024(4) Å, V = 7189.0(2) Å^3, Z = 8 (Table S1, ESI†). The crystallographic asymmetric unit of **1** contains three $[AOEMIm]^+$ cations and one isolated $[SbCl_6]^{3-}$ anion (Fig. 1a). It could be seen that the bond length of Sb–Cl in $[SbCl_6]^{3-}$ ranges from 2.549(3) to 2.809(4) Å, forming a distorted octahedral geometry (Table S2, ESI†). In addition, there are abundant weak interactions in the structure, such as C–H···Cl, C–O···H, and C–H···π (Fig. S4a–c, ESI†). The anionic unit $[SbCl_6]^{3-}$ formed a two-dimensional anionic layered structure through hydrogen bonding C–H···Cl (Fig. S4d, ESI†). The two-dimensional anionic layer formed a three-dimensional supramolecular framework by connecting the cationic layer through C–O···H and C–H···π (Fig. 1d, and Fig. S4e, ESI†).

2 crystallizes in a trigonal crystal system with the space group of $R\bar{3}$ and the cell parameters are a = 21.8818(4) Å, b = 21.8818(4) Å, c = 8.6170(3) Å, V = 3573.2(2) Å^3, Z = 3 (Table S1, ESI†). Its crystallographic asymmetric unit contains one half-deprotonated $[H_{0.5}OOCMMIm]^{+0.5}$ and one-sixth of a $[SbCl_6]^{3-}$ unit (Fig. 1b). That is, due to disorder, the organic moiety is composed of 0.5 $[HOOCMMIm]^+$ and 0.5 neutral [OOCMMIm] (Fig. S5b, ESI†). The anion is close to that of an *ortho*-octahedron, and the lengths of the six Sb–Cl bonds are similar so that of the anionic unit located on a threefold rotation (Fig. S5a, ESI†). Each anionic unit $[SbCl_6]^{3-}$ is surrounded by six imidazole rings with C–H···Cl h-bond interactions, forming a one-dimensional tubular structure (Fig. S5e, ESI†). Then the tubular structures are further interacted with each other *via* C–O···H and π···π interactions to form an overall three-dimensional supramolecular framework (Fig. 1e, and Fig. S5c, d, f, ESI†).

3 crystallizes in a monoclinic system with the space group of $P2_1/c$ and the cell parameters are a = 20.7233(11) Å, b = 8.7393(3) Å, c = 17.6064(9) Å, β = 114.637(6) °, V = 2898.4(3) Å^3, Z = 4 (Table S1, ESI†). The crystallographic asymmetric unit of **3** contains three $[HOOCMMIm]^+$ cations and one isolated $[SbCl_6]^{3-}$ anion (Fig. 1c). Notably, the Sb–Cl(6) bond with a bond length of 3.3245(7) Å, which is longer than the other Sb–Cl bonds, is seen as a secondary bond and results in an irregular octahedral anion (Table S2, ESI†). The anionic units form a two-dimensional anionic layer structure through hydrogen bonding C–H···Cl, and then the C–H···π and C–O···H interactions between the cations connected the two-dimensional anionic layer to form a three-dimensional supramolecular framework (Fig. 1f, and Fig. S6, ESI†).

Elemental analysis (EA) and PXRD results indicate that **1**, **2**, and **3** are pure phases (Fig. S7, ESI†). In addition, the ^{1}H NMR spectra of **2** and **3** show a characteristic peak of COOH at the

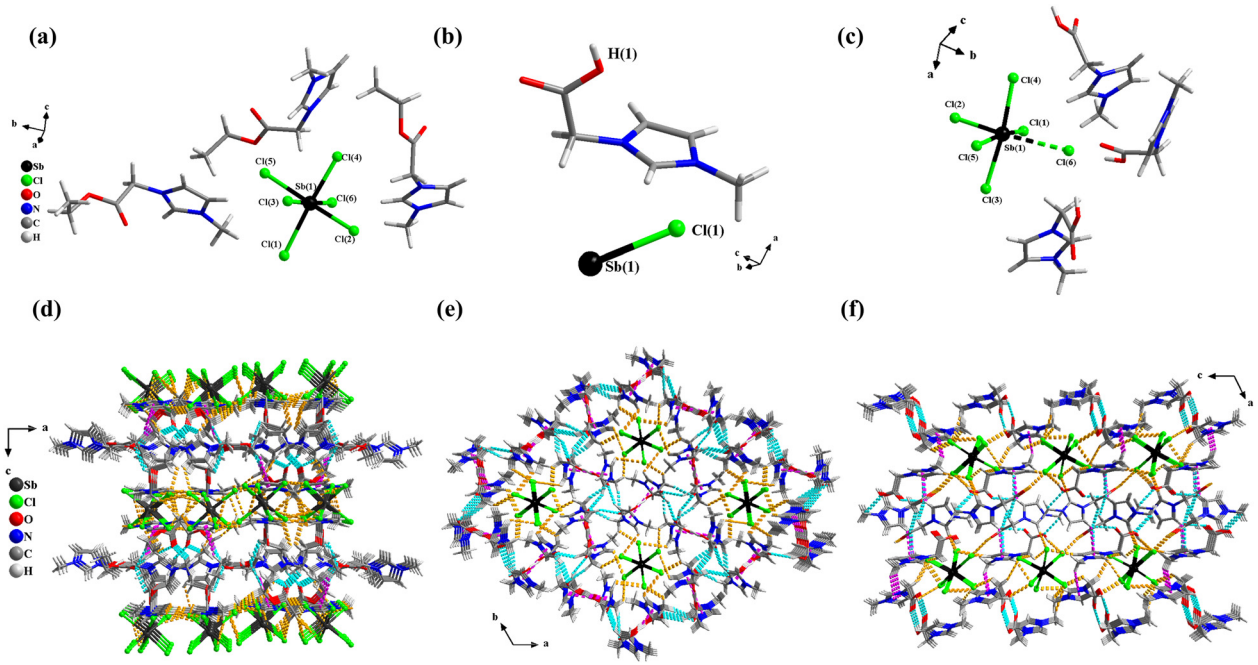

Fig. 1 (a)–(c) Asymmetric units of crystals **1**, **2** and **3**, respectively. H (1) is half-occupied in **2**. (d) The packing diagram of crystal **1** along the *b*-axis. (e) The packing diagram of crystal **2** along the *c*-axis. (f) The packing diagram of crystal **3** along the *b*-axis. The purple dashed lines represent cation···π interactions and π··· π interactions, the gold dashed lines represent C–H···Cl bonds, and the cyan dashed lines represent C–O···H bonds.

chemical shift of 12.50 ppm position. However, the COOH peak in **3** is much stronger than that in **2** (Fig. S8, ESI†), which is in good agreement with their structural components. Thermogravimetric (TG) analysis showed that **1**, **2** and **3** are stable below 250 °C, 240 °C and 160 °C, respectively. This indicates that the title compounds have good thermal stability, which lays a foundation for the subsequent study of fluorescence properties (Fig. S9, ESI†).

Luminescence properties

The photoluminescence (PL) spectra, photoluminescence excitation (PLE) spectra, and time-resolved PL spectra have been performed to investigate the photoluminescent properties of compounds **1**, **2** and **3**. The PL spectrum of **1** shows a main peak at 610 nm, while the main PLE peak is located at 365 nm with a shoulder peak at 292 nm. Similarly, **2** has a main PL peak at 510 nm with PLE peaks at 286 nm and 375 nm, while **3** has a main PL peak at 525 nm with PLE peaks at 280 nm and 345 nm (Fig. 2a–c). The two peaks of their PLE spectra should correspond to the $^1S_0 \rightarrow {}^1P_1$ and $^1S_0 \rightarrow {}^3P_1$ electronic transitions of Sb^{3+} ions, respectively.[48] The $^1S_0 \rightarrow {}^1P_1$ electronic transition was allowed, while the $^1S_0 \rightarrow {}^3P_1$ was partially allowed by the spin–orbit coupling.[3,49] **1**, **2** and **3** exhibit broadband peaks at 610, 510 and 525 nm under the excitation of 365 nm, 375 nm and 345 nm, respectively. The corresponding PL lifetimes for **1**, **2** and **3** are 3.168 μs, 2.093 μs and 3.106 μs (Fig. S10, ESI†), respectively, which suggests that their emissions might arise from the exciton relaxation of $^3P_n \rightarrow {}^1S_0$.[5] The PLQYs for **1**, **2** and **3** are 61.25%, 84.7% and 38.75%, respectively. The Commission Internationale del'Eclairage (CIE) chromaticity coordinates for **1**, **2** and **3** are (0.510, 0.460), (0.200, 0.435) and (0.293, 0.542), respectively (Fig. 2d).

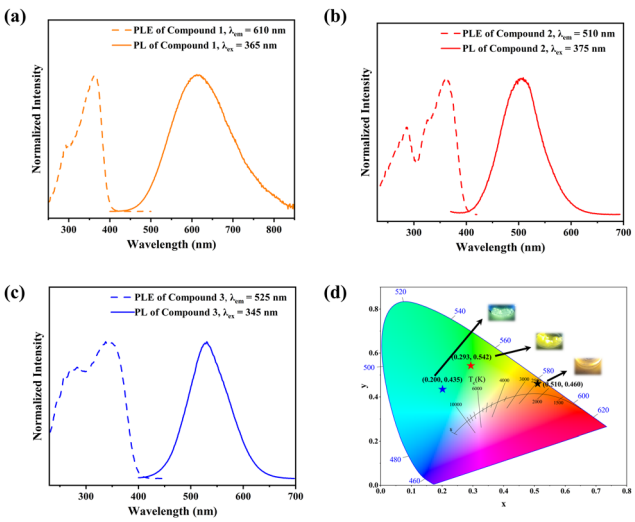

Fig. 2 **1** (a), **2** (b) and **3** (c) PLE and PL spectra at room temperature. The solid lines are the emission spectra at different excitation wavelengths. The dashed lines are the excitation spectra at different emission wavelengths. (d) CIE chromaticity coordinates corresponding to **1**, **2** and **3**. Inset: Photographs of the compounds under UV light.

The varied PLQYs of **1**, **2** and **3** might have a correlation with the distortion of $[SbCl_6]^{3-}$ in their crystal structure.[50,51] The lower the degree of ground state structural distortion, the stronger the symmetry of its structure, and the smaller the non-radiative excitation energy loss during the excited state

Table 1 Summary of the photophysical properties, σ^2 and Δd for the title compounds at 300 K

Compound	λ_{ex} (nm)	λ_{em} (nm)	FWHM (nm)	Φ (%)[a]	τ_{av} (μs)[b]	σ^2	Δd ($\times 10^{-4}$)	Ref.
$[AOEMIm]_3SbCl_6$ (1)	292, 365	610	170	61.25	3.168	6.50	13.07	This work
$[HOOCMMIm]_3SbCl_6 \cdot 3(OOCMMIm)$ (2)	286, 375	510	89	84.7	2.093	3.06	0	This work
$[HOOCMMIm]_3SbCl_6$ (3)	280, 345	525	90	38.75	3.106	16.94	117.61	This work

[a] Φ is the PLQY. [b] τ_{av} is the average PL lifetime.

recombination, thus increasing the possibility of stronger luminescence.[32] The distortions based on the Sb–Cl bond length and Cl–Sb–Cl angle variance are defined as follows.[52]

$$\sigma^2 = \frac{1}{11}\sum_{n=1}^{12}(\theta_n - 90^\circ)^2 \quad \text{(six coordinated)}$$

$$\Delta d = \frac{1}{6}\sum_{n=1}^{6}[(d_n - d)/d]^2 \quad \text{(six coordinated)}$$

where θ_n denotes the bond angle of each Cl–Sb–Cl, d_n is the average of the Sb–Cl bond distance, and d_n denotes individual Sb–Cl bond length. σ^2 and Δd represent the $[SbCl_6]^{3-}$ distortion level. The σ^2 values of $[SbCl_6]^{3-}$ in **1–3** were calculated as 6.50, 3.06 and 16.94, while the Δd ones are 13.07, 0 and 117.64, respectively (Table 1). The $[SbCl_6]^{3-}$ distortion level in **1–3** is inversely proportional to their PLQYs.

Structural transformation

It was noteworthy that the orange-emitting **1** and the yellow-green-emitting **3** can gradually convert into the green-emitting **2** when exposed to air, which is confirmed by the PXRD results (Fig. 3a and c). The transition time is determined by the relative humidity of the environment. The higher humidity will induce faster structural transformation from **3** to **2** (Fig. S11, ESI†). The ester group portion of $[AOEMIm]^+$ in **1** can be hydrolysed in air, resulting in irreversible conversion from **1** to **2** (eqn (1)). The conversion from **3** to **2** might be triggered by the H_2O-induced deprotonation from the carboxylate group to H_2O (Fig. 3b). To verify our speculation, we immersed **3** in acetonitrile and tested the pH before and after the structure transformation from **3** to **2** (Fig. S12, ESI†). The pH value changes from 5 to 2 (Fig. S13, ESI†), confirming the proton transfer in the transformation. During the transformation from **3** to **2**, $SbCl_3$ as a by-product is found in PXRD as shown in Fig. S14, ESI,† confirming the release of $SbCl_3$ during the transformation process

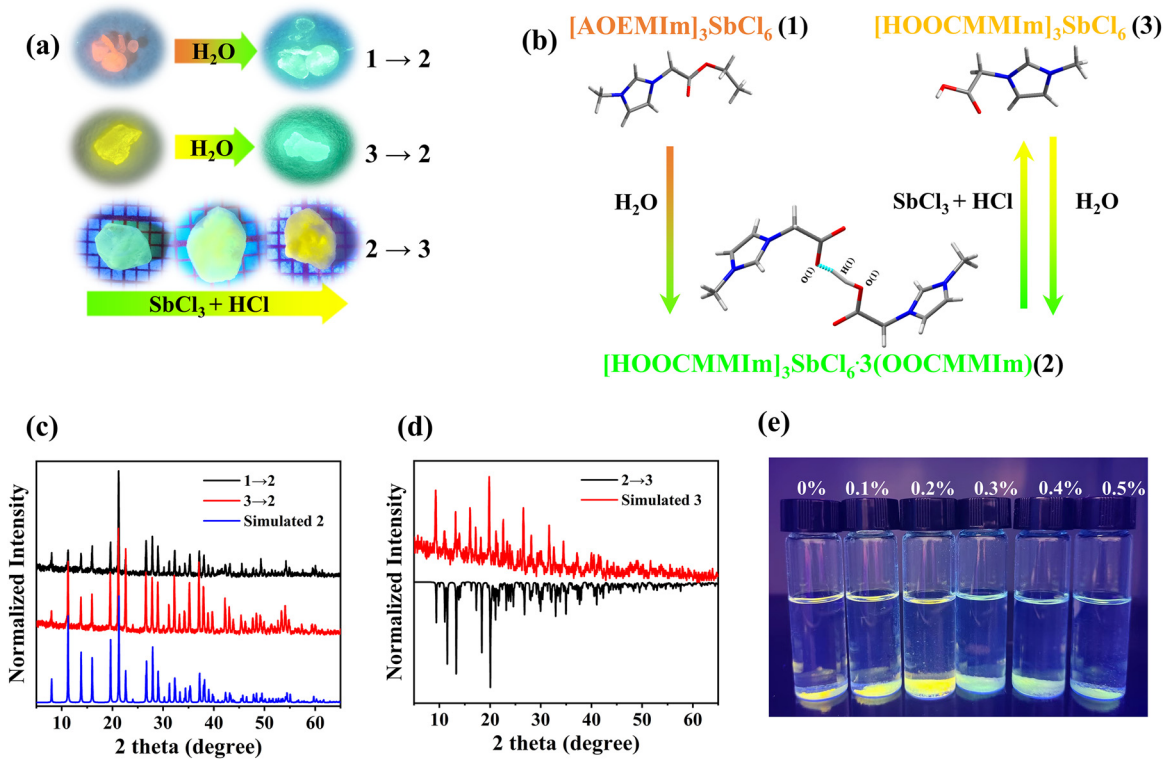

Fig. 3 (a) Plot of the transformations of the title compounds over time under UV irradiation. (b) Simple schematic of three-mode conversion. (c) Comparison of the experimental PXRD of **1** and **3** converted to **2** with the SCXRD simulation data of **2**, respectively. (d) Comparison of the experimental PXRD of **2** converted to **3** with the SCXRD simulated data of **3**. (e) Dehydration of **3** in tetrahydrofuran solvent containing different amounts of water (0–0.5% v/v).

(eqn (2)). Furthermore, based on eqn (3), **3** can be yielded by fumigating **2** with a mixture of $SbCl_3$ and HCl, which is confirmed by our experiments as shown in Fig. 3a, and d and Fig. S15 (ESI†). The structure transformations in this work are given as eqn (1) to eqn (3):

$$2[AOEMIm]_3SbCl_6\ (\mathbf{1}) + 9H_2O \rightarrow [HOOCMMIm]_3SbCl_6{\cdot}3(OOCMMIm)\ (\mathbf{2}) + 3H_3O^+ + SbCl_3 + 3Cl^- + 6CH_3CH_2OH \quad (1)$$

$$2[HOOCMMIm]_3SbCl_6\ (\mathbf{3}) + 3H_2O \rightarrow [HOOCMMIm]_3SbCl_6{\cdot}3(OOCMMIm)\ (\mathbf{2}) + 3H_3O^+ + SbCl_3 + 3Cl^- \quad (2)$$

$$[HOOCMMIm]_3SbCl_6{\cdot}3(OOCMMIm)\ (\mathbf{2}) + SbCl_3 + 3HCl \rightarrow 2[HOOCMMIm]_3SbCl_6\ (\mathbf{3}) \quad (3)$$

As far as we know, this is the first report about regulating the structure transition in IOMHs based on post-synthetic modification of the organic component.

Luminescent water-sensing

Various types of sensors have been used for water detection,[19,23,53,54] including fibre optic sensors, fluorescent sensors, capacitive sensors, and resistive sensors. The water triggers structural transformation and accordingly luminescence colour and/or intensity changes allow IOMHs to be used as fluorescence sensors.[22,23,27,28] Therefore, it can be applied to the detection of trace water in organic solvents,[55–57] which has the advantages of low cost, high sensitivity and so on. The powder of **3** was immersed in THF with different water contents (0–0.5% v/v). When the water content was above 0.3% v/v, the yellow-green emission of compound **3** turned into the green emission of compound **2** within 10 min. The detection limit of $[HOOCMMIm]_3SbCl_6$ was about 0.3% v/v (Fig. 3e), which was much lower than that of $(PPZ)_2SbCl_7{\cdot}5H_2O$ (1.5% v/v).[58]

Conclusion

In summary, three 0-D antimony (III) chloride-based IOHMs with photoluminescence from Sb(III) were synthesized by ionothermal and solventothermal methods. The single-crystal structures of these compounds are analysed in detail. The PLQYs of **1**, **2**, and **3** are 61.25%, 84.7%, and 38.75%, respectively, in correlation with the distortion of $[SbCl_6]^{3-}$ in their crystal structure. Under H_2O treatment, the ester group portion of $[AOEMIm]^+$ in **1** will be hydrolysed, while the carboxyl in **3** will be deprotonated. As a result, H_2O stimulated organic cation reconstruction can lead to the gradual and controllable transformation from **1** or **3** to **2**. In addition, stimulated by the vapour from HCl and $SbCl_3$, **2** is reversibly converted to **3**. The mechanism for the structural transformations among the title compounds is verified by experiments including PXRD and pH test. The H_2O triggered PL switching from **3** to **2** is adopted to detect the trace water in organic solvents. The water detection limit in THF is as low as 0.3% v/v, better than the previous homogeneous materials. This study opens a new avenue for synthesizing stimuli-responsive IOMHs through organic group reconstruction.

Experimental

Materials and methods

1-Acetoxyethyl-3 methylimidazolium chloride ([AOEMIm]Cl, 99%) and 1-carboxymethyl-3-methylimidazolium chloride ([HOOCMMIm]Cl, 99%) were purchased from Lanzhou Greenchem ILs (Lanzhou China); antimony (III) chloride ($SbCl_3$, 99%) was purchased from Adamas Reagent Co., Ltd. Methanol (CH_3OH, AR) was purchased from Sinopharm Chemical Reagent Co., Ltd (China). Tetrahydrofuran (THF, water ≤ 30 ppm (by K. F.), 99.9%, stabilized with BHT, SafeDry, Safeseal) was purchased from Adamas Reagent Co., Ltd. All reagents were used without further purification.

Characterization

Powder X-ray diffraction (PXRD) patterns were measured on a Rigaku Miniflex-II diffractometer by utilizing CuK_α radiation (λ = 1.54178 Å) in the angular range of 2θ = 5–65°.[59] Thermogravimetric (TG) analyses were performed on a NETZSCH STA 449F3 unit at a heating rate of 10 K min^{-1} under a N_2 atmosphere. Photoluminescence excitation (PLE) and photoluminescence (PL) spectra and time-resolved PL spectra and quantum yields of compound **1–3** were recorded on an Edinburgh FLS1000 UV/V/NIR fluorescence spectrometer. Elemental analysis (EA) was conducted on a German Elementary Vario MICRO instrument. Solid-state NMR spectra were obtained on a Bruker AVANCE III 500 M spectrometer.

Syntheses $[AOEMIm]_3SbCl_6$ (1)

The pure phase **1** was formed by the reaction of $SbCl_3$ and [AOEMIm]Cl with a molecular ratio of 1 : 3. The mixture was heated and dissolved to form a clear melt, which was then cooled to room temperature (RT) for 1 week to form colourless, transparent crystals. The yield was calculated to be nearly 52.7% based on the Sb atom. EA: calcd (%): C, 34.23%; H, 4.67%; N, 9.98%; found: C, 34.97%; H, 4.77%; N, 11.09%.

$[HOOCMMIm]_3SbCl_6{\cdot}3(OOCMMIm)$ (2)

The pure phase **2** was formed by the reaction of $SbCl_3$ and [HOOCMMIm]Cl in a molecular ratio of 1 : 6 and using 1 mL of methanol as a solvent. After reacting at RT for 10 hours, crystals of **2** would be formed. The yield was calculated to be nearly 63.0% based on the Sb atom. EA: calcd (%): C, 36.69%; H, 4.36%; N, 14.26%; found: C, 36.23%; H, 4.52%; N, 13.94%. ^1H NMR (500 MHz, δ): 3.81(s, 5H), 5.13(s, 5H), 6.79(s, 3H), 7.52(s, 4H), 8.93(s, 2H).

$[HOOCMMIm]_3SbCl_6$ (3)

3 was synthesized in a similar way to **2** with the mole ratio changed to 1 : 3. The mixture was heated to 80 °C for 10 hours so that it was clearly molten, and then crystals of **3** were

generated after cooling the molten mixture to room temperature (RT) for 1 day. The yield was calculated to be nearly 96.0% based on the Sb atom. EA: calcd (%): C, 28.52%; H, 3.59%; N, 11.09%; found: C, 28.70%; H, 3.59%; N, 11.26%. ^{1}H NMR (500 MHz, δ): 3.81 (s, 1H), 5.13 (s, 5H), 6.20 (s, 3H), 7.47 (s, 4H), 8.89 (s, 2H), 12.5 (s, 6H).

Single crystal X-ray diffraction (SCXRD)

A suitable single crystal was selected under an optical microscope for SCXRD measurement. Intensity data for single crystals **1** and **3** were collected at 100 K using graphite monochromatic MoK_α radiation (λ = 0.71073 Å) on a Supernova CCD diffractometer. Single-crystal intensity data for **2** were collected at 100 K using graphite monochromatic CuK_α radiation (λ = 1.54178 Å) on a Supernova CCD diffractometer. The structure was solved by direct methods and refined by full-matrix least-squares on F^2 using the SHELX-2018 program package.[60] The hydrogen atoms connected to all C atoms were located at geometrically calculated positions. The non-hydrogen atoms were refined anisotropically.

Data availability

CCDC No. 2341218, 2344297, 2341219 contain the supplementary crystallographic data for this paper. The data can be obtained free of charge from The Cambridge Crystallographic Data Centre *via* **https://www.ccdc.cam.ac.uk/data_request/cif**.

Author contributions

Z. P. W., Y. L. and D. D. H. conceived the project. Y. L. and D. D. H. designed and performed most of the experiments. Y. L. and D. D. H. carried out PL, PLE, PL attenuation, TG, UV, XRD, and SCXRD experiments. H. W. L. and Z. Z. Z. helped with the experiments. Y. L. and D. D. H. wrote the manuscript. Z. P. W., X. Y. H. and K. Z. D. revised the manuscript. All authors discussed the results and commented on the manuscript; Z. P. W., X. Y. H. and K. Z. D. supervised the project.

Conflicts of interest

There are no conflicts to declare.

Acknowledgements

This work was supported by the National Natural Science Foundation of China (No. 92261115, 22205236 and 22373014) and the Natural Science Foundation of Fujian Province (No. 2022J05089).

Notes and references

1 T.-H. Zhuang, Y.-M. Lin, H.-W. Lin, Y.-L. Guo, Z.-W. Li, K.-Z. Du, Z.-P. Wang and X.-Y. Huang, *Molecules*, 2023, **28**, 2380.
2 Y. Jing, Y. Liu, M. Li and Z. Xia, *Adv. Opt. Mater.*, 2021, **9**, 2002213.
3 Y.-C. Peng, S.-H. Zhou, J.-C. Jin, T.-H. Zhuang, L.-K. Gong, H.-W. Lin, Z.-P. Wang, K.-Z. Du and X.-Y. Huang, *J. Phys. Chem. C*, 2022, **126**, 17381–17389.
4 Y.-C. Peng, J.-C. Jin, Q. Gu, Y. Dong, Z.-Z. Zhang, T.-H. Zhuang, L.-K. Gong, W. Ma, Z.-P. Wang, K.-Z. Du and X.-Y. Huang, *Inorg. Chem.*, 2021, **60**, 17837–17845.
5 Y.-C. Peng, H.-W. Lin, S.-H. Zhou, J.-C. Jin, T.-H. Zhuang, A. Ablez, Z.-P. Wang, K.-Z. Du and X.-Y. Huang, *Molecules*, 2023, **28**, 1978.
6 K. M. McCall, V. Morad, B. M. Benin and M. V. Kovalenko, *ACS Mater. Lett.*, 2020, **2**, 1218–1232.
7 L. Zhou, J. F. Liao and D. B. Kuang, *Adv. Opt. Mater.*, 2021, **9**, 2100544.
8 J.-C. Jin, N.-N. Shen, Y.-P. Lin, L.-K. Gong, H.-Y. Tong, K.-Z. Du and X.-Y. Huang, *Inorg. Chem.*, 2020, **59**, 13465–13472.
9 J.-Q. Zhao, Y.-Y. Ma, X.-J. Zhao, Y.-J. Gao, Z.-Y. Xu, P.-C. Xiao, C.-Y. Yue and X.-W. Lei, *Research*, 2023, **6**, 0094.
10 S. Yu, H. Peng, Q. Wei, T. Li, W. Huang, X. He, Z. Du, J. Zhao and B. Zou, *Mater. Horiz.*, 2024, **11**, 2230–2241.
11 C. Sun, Y. H. Guo, S. S. Han, J. Z. Li, K. Jiang, L. F. Dong, Q. L. Liu, C. Y. Yue and X. W. Lei, *Angew. Chem., Int. Ed.*, 2020, **59**, 16465–16469.
12 C. Sun, J. Zang, Y. Liu, Q. Zhong, X. Xing, J. Li, C. Yue and X. Lei, *CCS Chem.*, 2022, **4**, 3106–3121.
13 J. Q. Zhao, M. F. Han, X. J. Zhao, Y. Y. Ma, C. Q. Jing, H. M. Pan, D. Y. Li, C. Y. Yue and X. W. Lei, *Adv. Opt. Mater.*, 2021, **9**, 2100556.
14 C. Zhou, L. J. Xu, S. Lee, H. Lin and B. Ma, *Adv. Opt. Mater.*, 2020, **9**, 2001766.
15 Y. Zhou and N. P. Padture, *ACS Energy Lett.*, 2017, **2**, 2166–2176.
16 N. X. Wu, C. Chen, S. T. Lin, H. H. Li, P. P. He and H. D. Zheng, *Inorg. Nano-Met. Chem.*, 2023, **53**, 428–436.
17 N. Leblanc, N. Mercier, M. Allain, O. Toma, P. Auban-Senzier and C. Pasquier, *J. Solid State Chem.*, 2012, **195**, 140–148.
18 W. C. Zhang, Z. H. Sun, J. Zhang, S. G. Han, C. M. Ji, L. N. Li, M. C. Hong and J. H. Luo, *J. Mater. Chem. C*, 2017, **5**, 9967–9971.
19 D. Y. Li, J. H. Song, Y. Cheng, X. M. Wu, Y. Y. Wang, C. J. Sun, C. Y. Yue and X. W. Lei, *Angew. Chem., Int. Ed.*, 2022, **61**, e202206437.
20 J. Q. Zhao, H. S. Shi, L. R. Zeng, H. Ge, Y. H. Hou, X. M. Wu, C. Y. Yue and X. W. Lei, *Chem. Eng. J.*, 2022, **431**, 134336.
21 Q. Kong, X. Meng, S. Ji, Q. Wang, B. Yang, T. Bai, X. Wang, Z. Wang, R. Zhang, D. Zheng, F. Liu and K.-L. Han, *ACS Mater. Lett.*, 2022, **4**, 1734–1741.
22 Z. Gong, W. Zheng, P. Huang, X. Cheng, W. Zhang, M. Zhang, S. Han and X. Chen, *Nano Today*, 2022, **44**, 101460.
23 W. Gao, M. Leng, Z. Hu, J. Li, D. Li, H. Liu, L. Gao, G. Niu and J. Tang, *Dalton Trans.*, 2020, **49**, 5662–5668.
24 Z. Wang and X. Huang, *Chem. – Eur. J.*, 2022, **28**, e202200609.

25 D.-Y. Li, J.-H. Song, Z.-Y. Xu, Y.-J. Gao, X. Yin, Y.-H. Hou, L.-J. Feng, C.-Y. Yue, H. Fei and X.-W. Lei, *Chem. Mater.*, 2022, **34**, 6985–6995.
26 S. Guo, Y. Zhao, K. Bu, Y. Fu, H. Luo, M. Chen, M. P. Hautzinger, Y. Wang, S. Jin, W. Yang and X. Lü, *Angew. Chem., Int. Ed.*, 2020, **59**, 17533–17539.
27 G. Song, M. Li, S. Zhang, N. Wang, P. Gong, Z. Xia and Z. Lin, *Adv. Funct. Mater.*, 2020, **30**, 2002468.
28 L. Zhou, J. F. Liao, Z. G. Huang, J. H. Wei, X. D. Wang, W. G. Li, H. Y. Chen, D. B. Kuang and C. Y. Su, *Angew. Chem., Int. Ed.*, 2019, **58**, 5277–5281.
29 O. Toma, M. Allain, F. Meinardi, A. Forni, C. Botta and N. Mercier, *Angew. Chem., Int. Ed.*, 2016, **55**, 7998–8002.
30 M.-M. Lun, H.-F. Ni, Z.-X. Zhang, J.-Y. Li, Q.-Q. Jia, Y. Zhang, Y. Zhang and D.-W. Fu, *Angew. Chem., Int. Ed.*, 2023, **63**, e202313590.
31 L. Gong, F. Huang, Z. Zhang, Y. Zhong, J. Jin, K.-Z. Du and X. Huang, *Chem. Eng. J.*, 2021, **424**, 130544.
32 M.-E. Sun, Y. Li, X.-Y. Dong and S.-Q. Zang, *Chem. Sci.*, 2019, **10**, 3836–3839.
33 H. L. Liu, H. Y. Ru, M. E. Sun, Z. Y. Wang and S. Q. Zang, *Adv. Opt. Mater.*, 2021, **10**, 2101700.
34 Y. Tian, H. Peng, Q. L. Wei, Y. X. Chen, J. J. Xia, W. C. Lin, C. Y. Peng, X. F. He and B. S. Zou, *Chem. Eng. J.*, 2023, **458**, 141436.
35 Z. An, R. M. Liao, H. Q. Yao, Y. Cheng, B. J. Zhu, J. R. Li and H. Y. Ye, *Eur. J. Inorg. Chem.*, 2023, **26**, e202200740.
36 J. Q. Zhao, Y. Y. Ma, X. J. Zhao, Y. J. Gao, Z. Y. Xu, P. C. Xiao, C. Y. Yue and X. W. Lei, *Research*, 2023, **6**, 0094.
37 X. He, H. Peng, Q. Wei, Z. Zhou, Z. Du, J. Zhao and B. Zou, *Aggregate*, 2024, **5**, e407.
38 W. Ma, Q. Qian, S. M. H. Qaid, S. Zhao, D. Liang, W. Cai and Z. Zang, *Nano Lett.*, 2023, **23**, 8932–8939.
39 K. J. Liu, K. Liu, S. Q. Hao, A. Hou, J. D. Cao, M. Z. Quan, Y. G. Wang, C. Wolverton, J. Zhao and Q. L. Liu, *Adv. Funct. Mater.*, 2024, **34**, 2309296.
40 S. H. Xue, C. M. Shi, L. J. Xu and Z. N. Chen, *Adv. Opt. Mater.*, 2024, 2302854.
41 Y. R. Xie, J. T. Peng, Q. Y. Qin and B. B. Luo, *ACS Appl. Nano Mater.*, 2024, **7**, 1319–1326.
42 B. Lian, J. D. Yao, M. Ren, B. S. Zou, B. B. Luo and R. S. Zeng, *J. Mater. Chem. C*, 2024, **12**, 2944–2952.
43 Y. Shi, Z. Ma, D. Zhao, Y. Chen, Y. Cao, K. Wang, G. Xiao and B. Zou, *J. Am. Chem. Soc.*, 2019, **141**, 6504–6508.
44 N. Shen, J. Li, G. Li, B. Hu, J. Li, T. Liu, L. Gong, F. Huang, Z. Wang and X. Huang, *Inorg. Chem.*, 2019, **58**, 8079–8085.
45 B. Yang, W. Ming, M. H. Du, J. K. Keum, A. A. Puretzky, C. M. Rouleau, J. Huang, D. B. Geohegan, X. Wang and K. Xiao, *Adv. Mater.*, 2018, **30**, 1705801.
46 Z. Zhang, Y. Lin, J. Jin, L. Gong, Y. Peng, Y. Song, N. Shen, Z. Wang, K. Du and X. Huang, *Angew. Chem., Int. Ed.*, 2021, **60**, 23373–23379.
47 F. Lin, H. Wang, H. Lin, W. Liu and J. Li, *Chem. Commun.*, 2021, **57**, 1754–1757.
48 A. Vogler and H. Nikol, *Comments Inorg. Chem.*, 1993, **14**, 245–261.
49 Z. Li, Y. Li, P. Liang, T. Zhou, L. Wang and R.-J. Xie, *Chem. Mater.*, 2019, **31**, 9363–9371.
50 D. Chen, F. Dai, S. Hao, G. Zhou, Q. Liu, C. Wolverton, J. Zhao and Z. Xia, *J. Mater. Chem. C*, 2020, **8**, 7322–7329.
51 A. Biswas, R. Bakthavatsalam, B. P. Mali, V. Bahadur, C. Biswas, S. S. K. Raavi, R. G. Gonnade and J. Kundu, *J. Mater. Chem. C*, 2021, **9**, 348–358.
52 G. V. G. K. Robinson and P. H. Ribbe, *Science*, 1971, **172**, 567–570.
53 J. B. Luo, J. H. Wei, Z. Z. Zhang and D. B. Kuang, *Inorg. Chem.*, 2022, **61**, 338–345.
54 M. Li, J. Zhou, M. S. Molokeev, X. Jiang, Z. Lin, J. Zhao and Z. Xia, *Inorg. Chem.*, 2019, **58**, 13464–13470.
55 H. S. Jung, P. Verwilst, W. Y. Kim and J. S. Kim, *Chem. Soc. Rev.*, 2016, **45**, 1242–1256.
56 P. Kumar, A. Ghosh and D. A. Jose, *ChemistrySelect*, 2021, **6**, 820–842.
57 D. Wang, H. Zhao, H. Li, S. Sun and Y. Xu, *J. Mater. Chem. C*, 2016, **4**, 11050–11054.
58 J.-B. Luo, J.-H. Wei, Z.-Z. Zhang and D.-B. Kuang, *Inorg. Chem.*, 2022, **61**, 338–345.
59 C. F. Macrae, I. Sovago, S. J. Cottrell, P. T. A. Galek, P. McCabe, E. Pidcock, M. Platings, G. P. Shields, J. S. Stevens, M. Towler and P. A. Wood, *J. Appl. Crystallogr.*, 2020, **53**, 226–235.
60 G. M. Sheldrick, *Acta Crystallogr., Sect. C: Struct. Chem.*, 2015, **71**, 3–8.

